

Compressive deformation of CoZr and (Co,Ni)Zr intermetallic compounds with B2 structure

MORHIKO NAKAMURA

National Research Institute for Metals, 1-2-1 Sengen, Tsukuba, Ibaraki 305, Japan

YOSHIO SAKKA

National Research Institute for Metals, 2-3-12 Nakameguro, Meguro-ku, Tokyo 153, Japan

B2 type (Co,Ni)Zr compounds which were prepared by arc-melting were deformed in compression at temperatures from liquid nitrogen temperature to 973 K. Their flow stress was anomalously dependent on the testing temperature, decreasing with increasing temperature up to room temperature and then increasing with temperature up to about 673 K, followed by a decrease. The peak of the flow stress was higher for PE specimens than for PA ones which were machined perpendicular and parallel to the direction of grain growth of the ingot, respectively. It is considered that this behaviour of the flow stress is caused, not by the phase transition but by the motion of superlattice dislocations. The ductility of CoZr was lowered by cracking at grain boundaries at which secondary phases were observed. The substitution of nickel for cobalt suppressed the grain boundary cracking and (Co,Ni)Zr had a higher ductility than CoZr.

1. Introduction

It is well known that some intermetallic compounds exhibit anomalous mechanical properties. Some of $L1_2$ type compounds such as Ni_3Al [1], Co_3Ti [2], $(Fe,Ni,Co)_3V$ [3] etc. show an unusual temperature dependence of their yield strength, that is, their yield strength increases with increasing temperature above room temperature. This behaviour is not expected for ordinary metals and alloys, and has been explained by an increase in cross slip of the superlattice dislocations from (111) planes to (100) planes as the temperature rises [4, 5]. A similar temperature dependence of the yield strength is observed in TiAl single crystals with $L1_0$ structure [6], but the mechanism of this behaviour has not been clarified.

The intermetallic compounds which exhibit a phase transition with increasing temperature sometimes exhibit a similar behaviour of the yield strength, that is, the yield strength has a peak around the transition temperature as the temperature rises. FeCo (B2 structure) exhibits the order-disorder transition at about 983 K and its yield strength has a peak just below the transition temperature [7]. NiTi (B2 structure) has the martensitic transformation at about room temperature and its yield strength increases with increasing temperature and has a peak at about 373 K [8]. CuZn (B2 structure) also exhibits an order-disorder transition at 748 K. Its yield strength increases with temperature up to 423–500 K and then decreases with increasing temperature [9, 10].

For B2 type intermetallic compounds like NiAl [11] which exhibit no order-disorder transition or martensitic transformation above room temperature, the

yield strength is considered to decrease monotonically with increasing temperature, although an increase in the yield strength of AgMg with increasing temperature was reported [12]. It is because the other report in which the yield strength of AgMg decreased monotonically with increasing temperature was also published [13]. Meanwhile, CoZr is the B2 type intermetallic compound of which ductility was improved by the addition of alloying element nickel [14], and CoZr is also reported to have no composition range for cobalt and zirconium [15]. However, the effect of testing temperature on the flow stress for this compound has not been studied, although the compressive yield strength is reported to increase just a little with temperature from room temperature to about 773 K [16], and the influence of nickel addition to CoZr on plastic deformation has not been examined.

In this paper, the effect of temperature on the flow stress of CoZr and (Co,Ni)Zr was examined using a compression test at temperatures from liquid nitrogen temperature to 973 K and the effect of nickel addition to CoZr on plastic deformation was also examined.

2. Experimental procedure

The intermetallic compounds were prepared by non-consumable arc-melting in an argon atmosphere using zirconium sheets which had been arc-melted using sponge zirconium, nickel sheets which had been vacuum melted using electrolytic nickel and electrolytic cobalt flakes. The arc-melted compounds of 100 g had the weight loss of less than 0.03%, so the chemical analyses of compositions were not carried out. The chemical compositions of raw materials are listed in

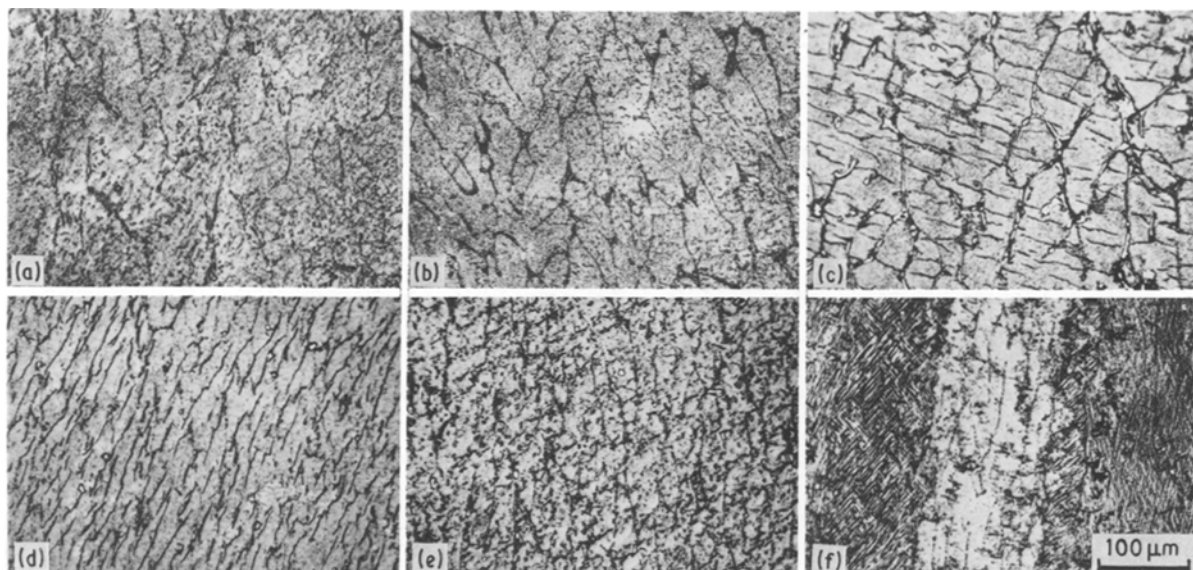


Figure 1 Microstructures of (a) $\text{Co}_{49.5}\text{Zr}_{50.5}$, (b) $\text{Co}_{50}\text{Zr}_{50}$, (c) $\text{Co}_{50.5}\text{Zr}_{49.5}$, (d) $\text{Co}_{48}\text{Ni}_2\text{Zr}_{50}$, (e) $\text{Co}_{45}\text{Ni}_5\text{Zr}_{50}$, and (f) $\text{Co}_{40}\text{Ni}_{10}\text{Zr}_{50}$.

Table I. The compounds were CoZr , $\text{Co}_{49.5}\text{Zr}_{50.5}$, $\text{Co}_{50.5}\text{Zr}_{49.5}$ and $\text{Co}_{50-x}\text{Ni}_x\text{Zr}_{50}$ ($x = 2 \sim 10$). The arc-melted materials were annealed at 1223 K for 180 ksec in vacuum for homogenizing, followed by machining compression specimens with a height of 6 mm and a cross sectional area of $2 \times 2 \text{ mm}^2$. The button shaped, arc-melted materials had the cast structure with large grains elongated parallel to the thickness direction and this structure was not eliminated by annealing at 1223 K for 180 ksec. Thus, both compression specimens with the height parallel to the thickness direction (PA specimen) and those with the height perpendicular to the thickness direction (PE specimen) were machined.

Compression tests were carried out using an Instron-type testing machine driven at a crosshead speed of 0.2 mm min ($5.6 \times 10^{-4} \text{ sec}^{-1}$) in the temperature range from liquid nitrogen temperature to 973 K. At above room temperature compression tests were conducted in vacuum after holding for 0.6 ksec at a given temperature. The average value of three specimens was generally adopted.

3. Experimental results

3.1. Microstructures of CoZr and $(\text{Co,Ni})\text{Zr}$

Fig. 1 shows the microstructures of $(\text{Co,Ni})\text{Zr}$, etc.

TABLE I Chemical compositions of raw materials

Raw material	Impurities (p.p.m.)
Zirconium sponge	Al < 50, B < 0.3, Cl < 240, Cr < 100, Co < 8, Fe = 450, Hf < 50, Mn < 20, N = 33, Ni < 10, O = 988, Pb < 15, Si < 60, Ti < 30, V < 20, Cd < 0.4, Cu < 10, C = 20, Mg = 264, W < 15, U < 1
Electrolytic cobalt (99.90 wt %)	Ni = 400, Fe = 40, Mn = 7, Cu = 15, Pb = 3, Zn = 30, Si = 10, S = 10, C = 50, H ₂ = 3, O ₂ = 70
Electrolytic nickel (Ni + Co > 99.95 wt %)	Co < 300, Fe < 50, Cu < 50, Pb < 10, Mn < 20, S < 10, Si < 500, C < 200

which were annealed at 1223 K for 180 ksec. The cast structure were observed for all the compounds. Although second phase particles were observed for stoichiometric compound CoZr , many more second phase particles were observed for cobalt-rich and nickel-rich non-stoichiometric compounds. The compounds in which cobalt was substituted by nickel showed similar structures to that of CoZr except for $\text{Co}_{40}\text{Ni}_{10}\text{Zr}_{50}$.

The structure change of these compounds with nickel addition was estimated using X-ray diffraction. Fig. 2 shows the ratio of integrated intensity of (100) diffraction to that of (200) diffraction for $\text{Co}_{50-x}\text{Ni}_x\text{Zr}_{50}$. This ratio represents the degree of order for B2 structure since the scattering factors of cobalt and nickel were approximately equal [17]. The degree of order was hardly influenced by an amount of substitutional nickel and heat treatment, i.e. annealing at 1223 K, quenching from 1223 K into ice water, and quenching followed by sub-zero cooling into liquid nitrogen.

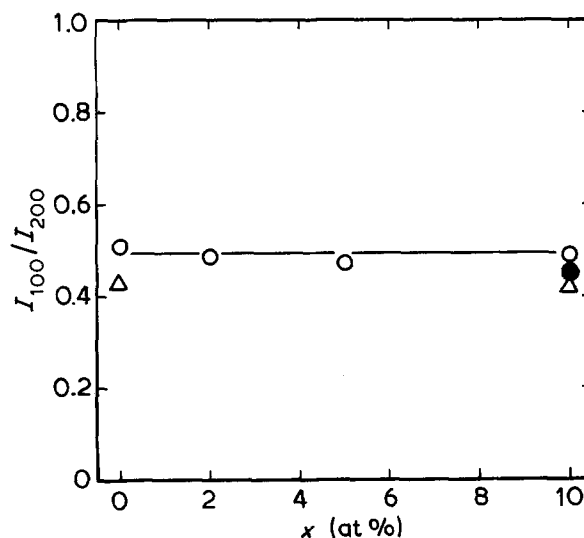


Figure 2 Dependence of the ratio of (200) integrated intensity to (100) intensity on content in $\text{Co}_{50-x}\text{Ni}_x\text{Zr}_{50}$. (○ as annealed, △ quenched, ● sub-zero cooled)

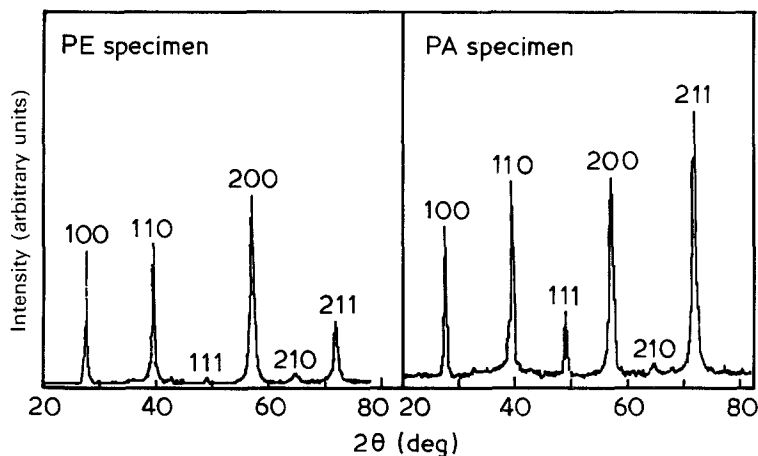


Figure 3 Diffraction patterns of PE and PA specimens of $\text{Co}_{50}\text{Zr}_{50}$.

In X-ray diffraction pattern of the longitudinal direction of PE specimens, $\{111\}$ and $\{211\}$ diffraction peaks were very small for all of the specimens, while in the case of PA specimens, $\{111\}$ and $\{211\}$ diffraction peaks of larger intensity were observed (Fig. 3). That is, PA specimens are considered approximately to have a preferred orientation of $[111] \sim [211]$ direction.

3.2. Mechanical properties of CoZr and (Co,Ni)Zr

Fig. 4 shows the effect of substitutional nickel on the flow stress for PE specimens of (Co,Ni)Zr at room temperature. The flow stress had a minimum value at nickel content of 2 at% and then increased with increasing nickel content for strains of 0.2%, 1% and 2%.

Fig. 5 shows the dependence of the compressive flow stress on temperature for PE specimens of $\text{Co}_{50}\text{Zr}_{50}$. The strength decreased with increasing

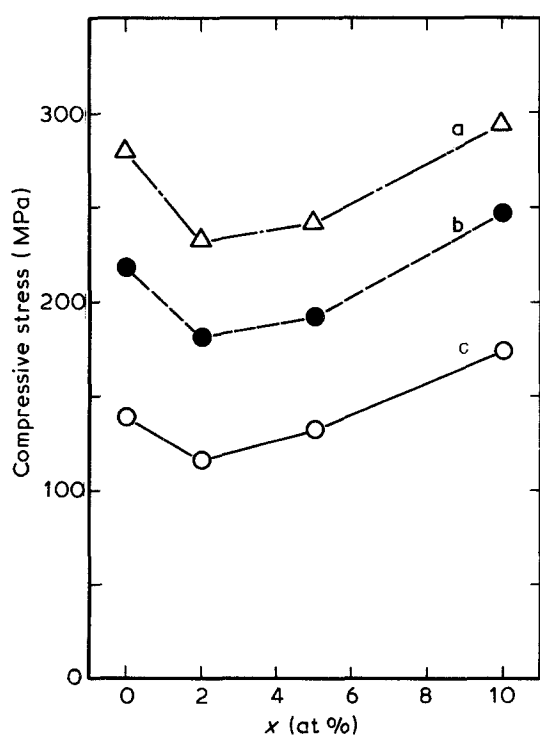


Figure 4 Dependence of the flow stress on nickel content for PE specimens, $\text{Co}_{50-x}\text{Ni}_x\text{Zr}_{50}$ tested at room temperature. (a) $\varepsilon = 2\%$, (b) $\varepsilon = 1\%$, (c) 0.2% .

temperature from liquid nitrogen temperature to room temperature and then increased with temperature up to about 673 K, followed by a further decrease with increasing temperature. The peak value of 0.2% offset stress was about twice as high as that at room temperature. The work hardening (i.e. a difference between 0.2% and 1% offset stresses) decreased with increasing temperature from 773 K, and at 973 K, CoZr hardly showed the work hardening at larger strain than 1%.

Fig. 6 shows the temperature dependence of the compressive flow stress for PE specimens of $\text{Co}_{48}\text{Ni}_2\text{Zr}_{50}$. The flow stress was largely decreased as the temperature rose from liquid nitrogen temperature to room temperature. Then, it increased with temperature up to 673 K and, consequently, had a peak at about 673 K as well as shown in Fig. 5. Fig. 7 also shows a similar dependence of the flow stress for PE specimens of $\text{Co}_{40}\text{Ni}_{10}\text{Zr}_{50}$. The flow stress at liquid nitrogen temperature was very high, which was caused by the martensitic transformation from B2 to B_f structure. The transformation from B_f to B2 structure was not perfectly obtained from liquid nitrogen temperature to room temperature (see Fig. 14) and then the flow stress for specimens sub-zero cooled to liquid nitrogen was considerably higher than that for as-annealed specimens at room temperature, that is, 0.2% offset stress was 490 MPa, 1% offset stress was 620 MPa, and 2% offset stress was 690 MPa. The flow stress increased

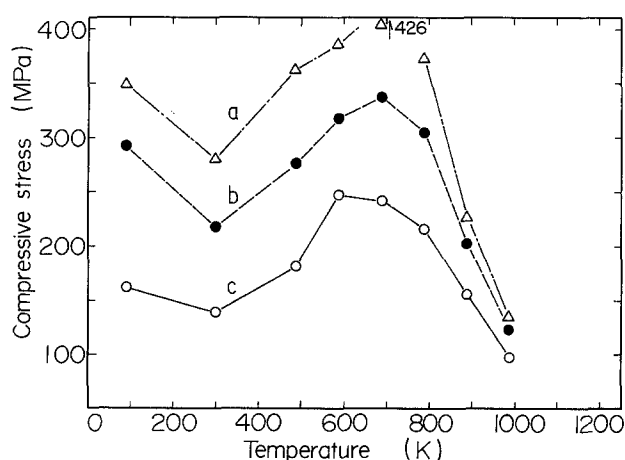


Figure 5 Temperature dependence of the flow stress in PE specimens of $\text{Co}_{50}\text{Zr}_{50}$. (a) $\varepsilon = 2\%$, (b) $\varepsilon = 1\%$, (c) 0.2% .

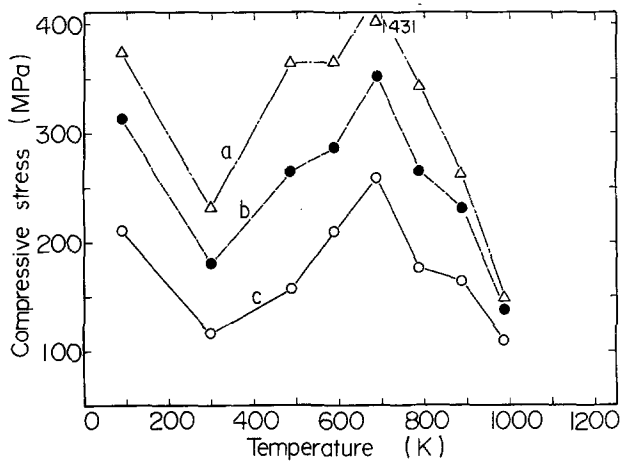


Figure 6 Temperature dependence of the flow stress in PE specimens of $\text{Co}_{48}\text{Ni}_2\text{Zr}_{50}$.

with temperature and had a peak value at about 673 K as well as shown for CoZr and $\text{Co}_{48}\text{Ni}_2\text{Zr}_{50}$. The peak value was about 1.4 times as high as the flow stress at room temperature and the increase of the flow stress was not so high as that for CoZr and $\text{Co}_{48}\text{Ni}_2\text{Zr}_{50}$. The flow stress at 973 K was approximately equal to that for CoZr and $\text{Co}_{48}\text{Ni}_2\text{Zr}_{50}$.

Fig. 8 shows the effect of temperature on the flow stress for PE specimens of $\text{Co}_{50.5}\text{Zr}_{49.5}$. Although all of the flow stresses were higher than those for the stoichiometric compounds, the behaviour of the flow stress was similar to that for $(\text{Co},\text{Ni})\text{Zr}$. The peak flow stress was obtained at about 573 K and an increase in the flow stress with increasing temperature was not so high as that for $(\text{Co},\text{Ni})\text{Zr}$. The flow stress of $\text{Co}_{49.5}\text{Zr}_{50.5}$ also showed a similar behaviour to that of $\text{Co}_{50.5}\text{Zr}_{49.5}$.

Fig. 9 shows the temperature dependence of 0.2% offset stress for PA specimens of $\text{Co}_{50}\text{Zr}_{50}$ and $\text{Co}_{45}\text{Ni}_5\text{Zr}_{50}$. In $\text{Co}_{50}\text{Zr}_{50}$, 0.2% offset stress was smaller for PA specimens than for PE ones. Although the 0.2% offset stress had a peak value at about 673 K, its peak height was much smaller, compared with that for PE specimens, and the peak stress was about 1.5 times as high as 0.2% offset stress at room temperature. In $\text{Co}_{45}\text{Ni}_5\text{Zr}_{50}$, 0.2% offset stress had a peak

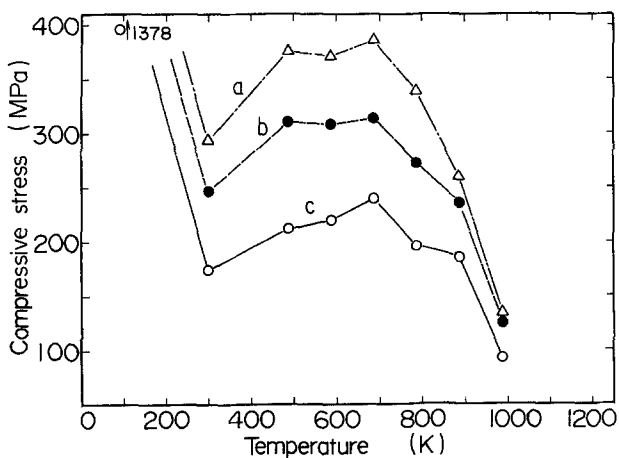


Figure 7 Temperature dependence of the flow stress in PE specimens of $\text{Co}_{40}\text{Ni}_{10}\text{Zr}_{50}$.

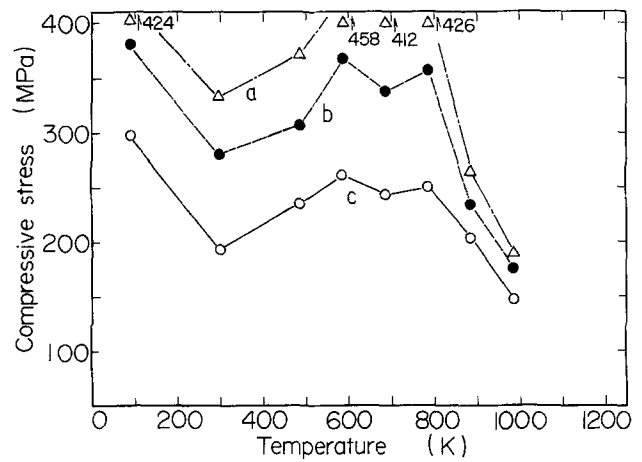


Figure 8 Temperature dependence of the flow stress in PE specimens of $\text{Co}_{50.5}\text{Zr}_{49.5}$.

value at about 773 K, and its increase with temperature was still smaller than that of PE specimens of $\text{Co}_{50}\text{Zr}_{50}$.

The strain rate dependence of the flow stress was examined by using the strain rate change method (Fig. 10). At temperatures below 673 K, the strain rate dependence was hardly observed, while at temperatures above 773 K, it became large. This behaviour is similar to that of CuZn polycrystals [9].

3.3. Microstructures of compressed specimens

Fig. 11 shows the microstructures of $\text{Co}_{50}\text{Zr}_{50}$ PE specimens which were compressed at various temperatures. The loading direction is the horizontal direction of the photographs. For the specimen deformed by about 10% at liquid nitrogen temperature, a cleavage crack with a length of about $100\ \mu\text{m}$ was observed in addition to grain boundary cracks. For specimens deformed by about 13% at temperatures from room temperature to 673 K, cracks were observed at grain boundaries, while cracks were hardly observed for specimens deformed at temperatures more than 773 K. $\text{Co}_{48}\text{Ni}_2\text{Zr}_{50}$ specimens also showed similar deformed microstructures to $\text{Co}_{50}\text{Zr}_{50}$.

Fig. 12 shows the microstructures of compressed PE specimens of $\text{Co}_{40}\text{Ni}_{10}\text{Zr}_{50}$. Cleavage-like cracks were

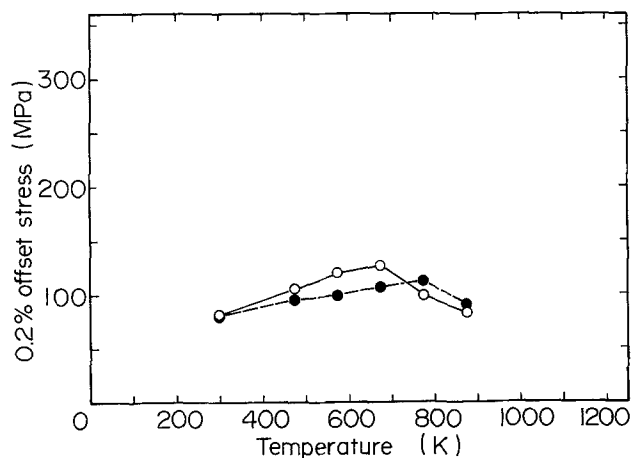


Figure 9 Temperature dependence of 0.2% offset stress in PA specimens of $\text{Co}_{50}\text{Zr}_{50}$ and $\text{Co}_{45}\text{Ni}_5\text{Zr}_{50}$. (O) $\text{Co}_{50}\text{Zr}_{50}$, (●) $\text{Co}_{45}\text{Ni}_5\text{Zr}_{50}$.

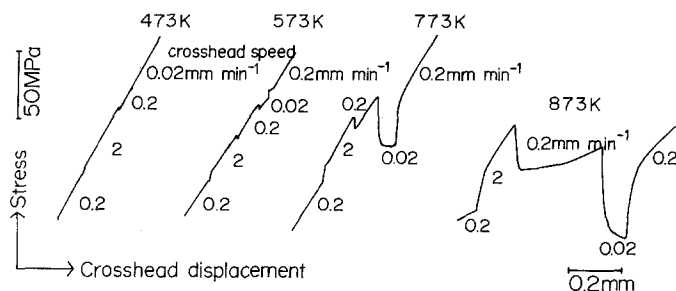


Figure 10 Change of the flow stress accompanied with strain rate change (PA specimens of $\text{Co}_{45}\text{Ni}_5\text{Co}_{50}$).

observed for specimens deformed at liquid nitrogen temperature. Grain boundary cracks which were obtained at above room temperature in other specimens (Fig. 11) were scarcely observed at above room temperature. When specimens sub-zero cooled to liquid nitrogen temperature were compressed at room temperature, cleavage cracks were also observed. That is, cleavage cracks which were obtained at liquid nitrogen temperature for annealed $\text{Co}_{40}\text{Ni}_{10}\text{Zr}_{50}$ and at room temperature for sub-zero cooled might be caused by deforming martensitic transformed structure. The appreciable amount of substitutional nickel for cobalt was found to suppress grain boundary cracking and to improve the ductility.

Fig. 13 shows the microstructures of compressed PE specimens of $\text{Co}_{49.5}\text{Zr}_{50.5}$ which has relatively large second phases. Many cracks are observed at grain boundaries. This observation indicates that the second phases along grain boundaries play an important role in cracking of deformed specimens. However, these cracks were not observed for specimens deformed at above 773 K. The microstructures of compressed $\text{Co}_{50.5}\text{Zr}_{49.5}$ were similar to those in Fig. 13.

4. Discussion

One of the characteristic deformation behaviours of B2 type CoZr or (Co,Ni)Zr compounds is the temperature dependence of the compressive flow stress. That is, the flow stress decreases with increasing temperature from liquid nitrogen temperature to room temperature and then increases with temperature up to about 673 K, followed by a further decrease.

An anomalous dependence of the flow stress on temperature was observed in some cases. The case

which must be considered first is the precipitation of second phases during heating for a compression test. Co-Zr phase diagram shows that CoZr has no composition range [15] and this fact is also reported by Suzuki *et al.* [18]. So, the precipitation of second phases during heating before testing is neglected. If second phases are precipitated during heating, an increase in the flow stress with temperature will change with heating time before testing. However, the heating time dependence of the flow stress was not observed. The fact that the peak height of the flow stress was higher for PE specimens than for PA ones may also give the evidence that the precipitation of second phases did not cause the anomalous behaviour of the flow stress, because both specimens were machined from the same ingot of the compound.

Next, the martensitic transformation must be considered. The anomalous temperature dependence of the flow stress of AuCd [19] and NiTi [13] was reported to be caused by the martensitic transformation. That is, the flow stress is lowered at about transformation temperature and increases with temperature up to a critical temperature (M_d), followed by a decrease again with increasing temperature. Although the $\text{Co}_{40}\text{Ni}_{10}\text{Zr}_{50}$ which is cooled to liquid nitrogen temperature, the martensitic transformation is observed by the measurement of electric resistivity [14], $\text{Co}_{50}\text{Zr}_{50}$ which is cooled to liquid nitrogen temperature is reported to have no transformation [14]. Compared with the flow stress at liquid nitrogen temperature for $\text{Co}_{40}\text{Ni}_{10}\text{Zr}_{50}$ and that at room temperature for $\text{Co}_{40}\text{Ni}_{10}\text{Zr}_{50}$ sub-zero cooled to liquid nitrogen temperature, the flow stress at liquid nitrogen temperature for $\text{Co}_{48}\text{Ni}_2\text{Zr}_{50}$ is much lower

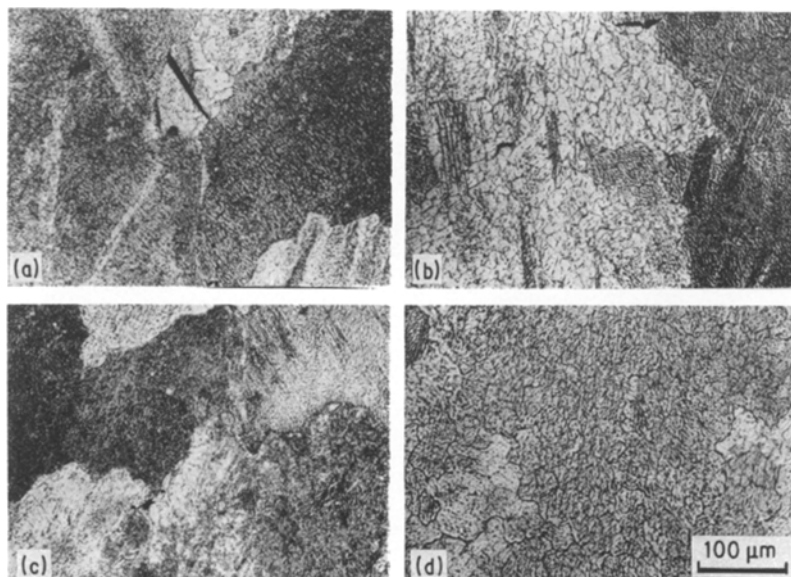


Figure 11 Microstructures of deformed specimens ($\text{Co}_{50}\text{Zr}_{50}$). Compressed at (a) liquid nitrogen temperature ($\epsilon = 10\%$), (b) room temperature ($\epsilon = 13\%$), (c) 673 K ($\epsilon = 13\%$), and (d) 973 K ($\epsilon = 25\%$).

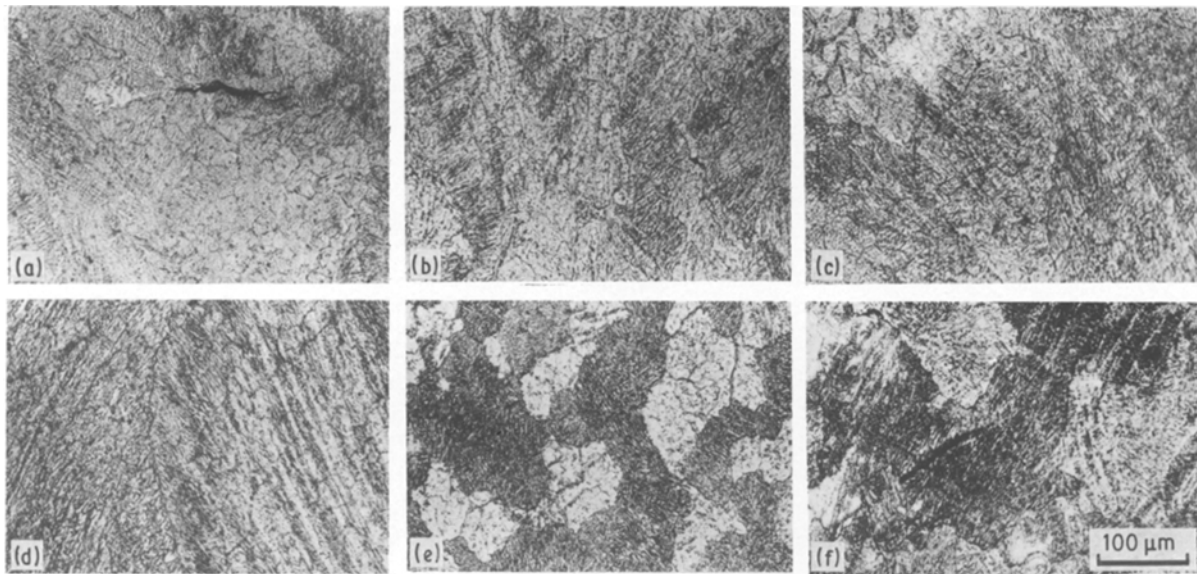


Figure 12 Microstructures of deformed specimens ($\text{Co}_{40}\text{Ni}_{10}\text{Zr}_{50}$). Compressed at (a) liquid nitrogen temperature ($\epsilon = 3\%$), (b) room temperature ($\epsilon = 18\%$), (c) 473 K ($\epsilon = 13\%$), (d) 673 K ($\epsilon = 15\%$), (e) 973 K ($\epsilon = 14\%$), and (f) room temperature (sub-zero cooled specimen, $\epsilon = 24\%$).

and it is considered that this compound has no martensitic transformation even when it is cooled to liquid nitrogen temperature. Meanwhile, the flow stress has a minimum value at about room temperature and a maximum value at about 673 K for CoZr and $\text{Co}_{48}\text{Ni}_2\text{Zr}_{50}$ (Figs 5 and 6). So, these facts indicate that the anomalous dependence of the flow stress on temperature is not caused by the martensitic transformation.

Thirdly, the order–disorder transition must be considered. The peak of the flow stress which is observed in the temperature dependence of the flow stress for FeCo [7], etc. is explained by the order–disorder transition [20]. It was confirmed by the measurement of the electric resistivity that CoZr has no order–disorder transition up to 1173 K [18]. The measurement of the thermal dilatation also showed the same result. Fig. 14 shows the thermal dilatation from room temperature to 1223 K for $(\text{Co}, \text{Ni})\text{Zr}$ and the result of FeCo was also shown in the same figure for comparison. In the dilatation–temperature curves of $(\text{Co}, \text{Ni})\text{Zr}$, the anomalous change of dilatation which is observed at the order–disorder transition temperature, i.e. about 980 K for FeCo , is not obtained. The anomalous dilatation which is observed at about 360 K during heating for sub-zero cooled $\text{Co}_{40}\text{Ni}_{10}\text{Zr}_{50}$ was caused by reverse transformation from B_f to B_2 structure, since $\text{Co}_{40}\text{Ni}_{10}\text{Zr}_{50}$ is transformed marten-

sitically from B_2 to B_f structure during sub-zero cooling. Therefore, the peak of the flow stress which was observed at about 673 K is not an increase in the flow stress caused by disordering of the compound at about the transition temperature.

Finally, the mechanism which is related to plastic deformation is considered. Three mechanisms are proposed for the positive temperature dependence of the yield strength in B_2 type CuZn . One is the model that a difference between antiphase boundary (APB) energy of moving superlattice dislocations and that of dislocations at thermal equilibrium produces an increase in yield strength [9, 21]. This model shows that the peak of the yield strength is related to the order–disorder transition, and cannot be applied to CoZr which has no order–disorder transition. The second one is the cross slip model that the increase of the yield strength is caused by the cross slip of superlattice screw dislocations from (110) to (112) plane with an increase in temperature [10], which is similar to the Kear–Wilsdorf mechanism for L_1_2 compounds [5]. However, the reason why the cross slip from (110) to (112) plane is produced is not clear, since the APB energy of the (112) plane is not lower than that of the (110) plane. Recently, the anomalous temperature dependence of the flow stress for CuZn has been explained by the slip motion of climb-dissociated superlattice dislocations [22, 23]. The climb-dissociated

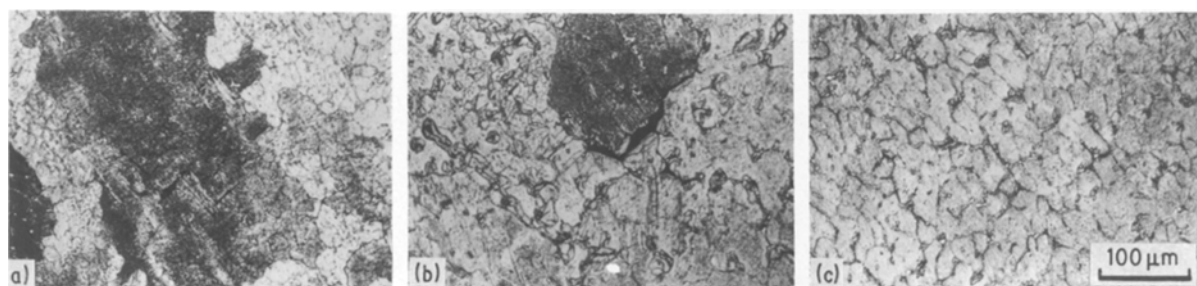


Figure 13 Microstructures of deformed specimens ($\text{Co}_{50.2}\text{Zr}_{49.5}$). Compressed at (a) liquid nitrogen temperature ($\epsilon = 8\%$), (b) 573 K ($\epsilon = 15\%$), and (c) 873 K ($\epsilon = 11\%$).

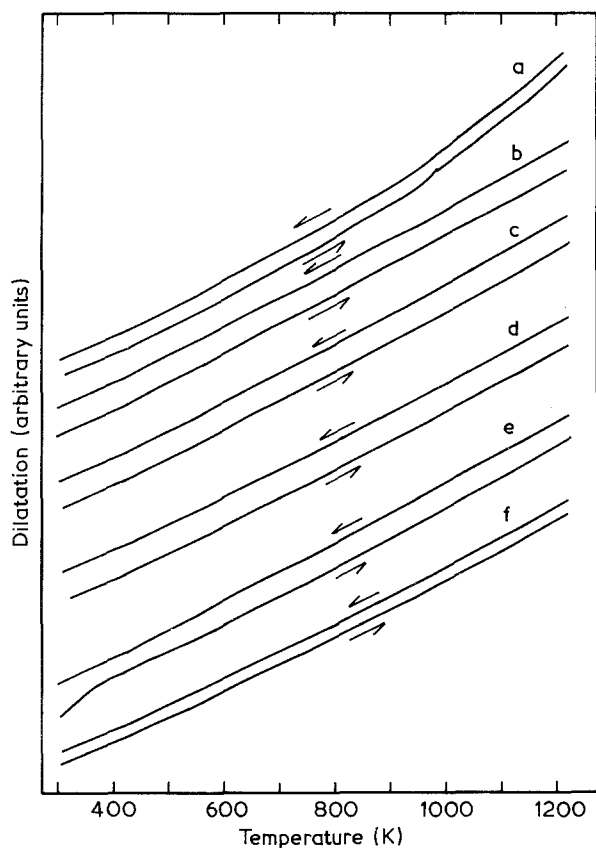


Figure 14 Thermal dilatation curves in the temperature range from room temperature to 1223 K. (a) FeCo, (b) CoZr, (c) $\text{Co}_{45}\text{Ni}_5\text{Zr}_{50}$, (d) $\text{Co}_{40}\text{Ni}_{10}\text{Zr}_{50}$, (e) $\text{Co}_{40}\text{Ni}_{10}\text{Zr}_{50}$ sub-zero cooled, (f) $\text{Co}_{50.5}\text{Zr}_{49.5}$.

dislocations which have antiphase boundaries on the non-slip planes were observed in the CuZn single crystal deformed at the temperature for the peak flow stress using the weak beam technique for an electron microscope [23]. A similar mechanism may be applied to the deformation of (Co,Ni)Zr, since (Co,Ni)Zr shows a similar strain rate dependence of the flow stress to CuZn (Fig. 10).

However, in order to propose a model explaining the temperature dependence of the flow stress for (Co,Ni)Zr, further investigations in which (Co,Zr)Ni single crystals are used will be necessary. That is, the determination of the slip system, the effect of crystal orientation on the loading axis on the anomalous flow stress behaviour, etc. need to be studied. The fact that the peak height of the flow stress is higher for PE specimens than for PA ones may indicate the orientation dependence of the flow stress, because the (111) peak of the X-ray diffraction pattern was scarcely observed for the former specimens but was distinguishable for the latter. The poor ductility of CoZr is caused by the secondary phases at grain boundaries, since the cracking was found at the grain boundaries at which the secondary phase was observed and was more frequently observed for off-stoichiometric compounds. The substitution of nickel for cobalt suppressed the grain boundary cracking which was observed for CoZr and improved the ductility. As the degree of order did not change with the content of nickel up to 10 at% as shown in Fig. 2, the improvement of ductility is not caused by the disordering of the B2 structure. It may

not be caused by the martensitic transformation, either, because the effect of nickel substitution appeared at above room temperature. Although substitutional nickel improved the strength of the grain boundaries, further study is necessary to clarify the effect of nickel on the ductility of CoZr.

4. Conclusion

B2 type (Co,Ni)Zr compounds which were prepared by non-consumable arc-melting were deformed in compression at temperatures from liquid nitrogen temperature to 973 K. Their flow stress was anomalously dependent on testing temperature. That is, it decreased with increasing temperature up to room temperature and then increased with temperature up to about 673 K, followed by a further decrease. The peak of the flow stress was higher for PE specimens than for PA ones. Here, the former and the latter specimens were machined perpendicular and parallel to the direction of grain growth of the ingot, respectively, and the height direction of PA specimens was found to have a preferred orientation of about $[111] \sim [211]$ by X-ray diffraction. The change of the flow stress which was caused by the strain rate change was hardly found at temperatures below the peak temperature, but the flow stress decreased largely with a decrease in strain rate at temperatures above the peak temperature. It is considered that this behaviour of the flow stress is caused not by the phase transition but by the slip motion of the superlattice dislocations. A model which explains this anomalous behaviour of the flow stress has not yet been given, although the mechanism which was proposed for CuZn may be applied to (Co,Ni)Zr. The ductility of CoZr was lowered by cracking at grain boundaries at which secondary phases were observed. The substitution of nickel for cobalt suppressed the grain boundary cracking and (Co,Ni)Zr had a higher ductility than CoZr.

Further investigation is necessary in order to clarify the deformation behaviour of B2 type (Co,Ni)Zr compounds.

References

1. P. H. THORNTON, R. G. DAVIES and T. L. JOHNSTON, *Met. Trans.* **1** (1970) 207–218.
2. T. TAKASUGI and O. IZUMI, *Acta Metall.* **33** (1985) 39–48.
3. C. T. LIU, *Int. Met. Rev.* **29** (1984) 168–194.
4. B. H. KEAR and H. G. WILSDORF, *Trans. Met. Soc. AIME* **224** (1962) 382–386.
5. S. TAKEUCHI and E. KURAMOTO, *Acta Metall.* **21** (1973) 415–425.
6. T. KAWABATA and O. IZUMI, *ibid.* **33** (1985) 1355–1366.
7. M. J. MARCINKOWSKI, *J. Inst. Met.* **93** (1963–1964) 476–480.
8. A. G. ROSNER and R. J. WASOLEWSKI, *J. Inst. Met.* **94** (1966) 169–175.
9. K. AOKI and O. IZUMI, *J. Jpn Inst. Met.* **36** (1972) 113–118 (in Japanese).
10. Y. UMAKOSHI, M. YAMAGUCHI, Y. NAMBA and K. MURAKAMI, *Acta Metall.* **24** (1976) 89–93.
11. R. T. PASCOE and C. W. A. NEWAY, *Met. Sci. J.* **2** (1968) 138–143.
12. A. K. MUKHERJEE, W. G. FERGUSON, W. L. BARMORE and J. E. DORN, *J. Appl. Phys.* **37** (1966) 3707–3713.

13. D. L. WOOD and J. H. WESTBROOK, *Trans. Met. Soc. AIME* **224** (1962) 1024-1037.
14. H. HOSSAIN, I. R. HARRIS and K. G. BARRACLOUGH, *J. Less-Common Met.* **37** (1974) 35-57.
15. R. P. ELLIOTT, "Constitution of Binary Alloys, First Supplement" (McGraw-Hill, New York, 1965) p. 344.
16. T. SUZUKI, PhD thesis, Tohoku University (1976).
17. B. D. CULLITY, "Elements of X-ray Diffraction", 2nd Edn (Addison-Wesley, Mass., 1978) Appendix 12.
18. T. SUZUKI and K. MASUMOTO, *J. Jpn Inst. Met.* **39** (1975) 117-121 (in Japanese).
19. N. NAKANISHI, *J. Cryst. Soc. Jpn* **14** (1972) 307-317 (in Japanese).
20. N. STOLOFF, "Strengthening Methods in Crystals", edited by A. Kelly and R. B. Nicholson (Elsevier, New York, 1971) 193-260.
21. N. BROWN, *Phil. Mag.* **4** (1959) 693-704.
22. P. A. FLINN, *Trans. Met. Soc. AIME* **218** (1960) 145-154.
23. H. SAKA and Y. M. ZHU, *Phil. Mag.* **A51** (1985) 629-637.

*Received 28 October 1987
and accepted 25 February 1988*